

Likelihood Approximation With Hierarchical Matrices For Large Spatial Datasets

Alexander Litvinenko *

Ying Sun, Marc G. Genton and David Keyes

King Abdullah University of Science and Technology, Thuwal 23955-6900, Saudi Arabia [†]

June 24, 2022

Abstract

We use available measurements to estimate the unknown parameters (variance, smoothness parameter, and covariance length) of a covariance function by maximizing the joint Gaussian log-likelihood function. To overcome cubic complexity in the linear algebra, we approximate the discretized covariance function in the hierarchical (\mathcal{H} -) matrix format. The \mathcal{H} -matrix format has a log-linear computational cost and storage $\mathcal{O}(kn \log n)$, where the rank k is a small integer and n is the number of locations. The \mathcal{H} -matrix technique allows us to work with general covariance matrices in an efficient way, since \mathcal{H} -matrices can approximate inhomogeneous covariance functions, with a fairly general mesh that is not necessarily axes-parallel, and neither the covariance matrix itself nor its inverse have to be sparse. We demonstrate our method with Monte Carlo simulations and an application to soil moisture data. The C, C++ codes and data are freely available.

Keywords: Computational statistics; Hierarchical matrix; Large dataset; Matérn covariance; Random Field; Spatial statistics.

1 Introduction

The number of measurements that must be processed for statistical modeling in environmental applications is usually very large, and these measurements may be located irregularly across a given geographical region. This makes the computing process expensive and the data difficult to manage. These data are frequently modeled as a realization from a stationary Gaussian spatial random field. Specifically, we let $\mathbf{Z} = \{Z(\mathbf{s}_1), \dots, Z(\mathbf{s}_n)\}^\top$, where $Z(\mathbf{s})$ is a Gaussian random field indexed by a spatial location $\mathbf{s} \in \mathbb{R}^d$, $d \geq 1$. Then, we assume that \mathbf{Z} has mean zero and a stationary parametric covariance function $C(\mathbf{h}; \boldsymbol{\theta}) = \text{cov}\{Z(\mathbf{s}), Z(\mathbf{s} + \mathbf{h})\}$, where $\mathbf{h} \in \mathbb{R}^d$ is a spatial lag vector

*Corresponding author

[†]E-mails: alexander.litvinenko{ying.sun, marc.genton, david.keyes}@kaust.edu.sa

and $\boldsymbol{\theta} \in \mathbb{R}^q$ is the unknown parameter vector of interest. Statistical inferences about $\boldsymbol{\theta}$ are often based on the Gaussian log-likelihood function:

$$\mathcal{L}(\boldsymbol{\theta}) = -\frac{n}{2} \log(2\pi) - \frac{1}{2} \log |\mathbf{C}(\boldsymbol{\theta})| - \frac{1}{2} \mathbf{Z}^\top \mathbf{C}(\boldsymbol{\theta})^{-1} \mathbf{Z}, \quad (1)$$

where the covariance matrix $\mathbf{C}(\boldsymbol{\theta})$ has entries $C(\mathbf{s}_i - \mathbf{s}_j; \boldsymbol{\theta})$, $i, j = 1, \dots, n$. The maximum likelihood estimator of $\boldsymbol{\theta}$ is the value $\hat{\boldsymbol{\theta}}$ that maximizes (1). When the sample size n is large, the evaluation of (1) becomes challenging, due to the computation of the inverse and log-determinant of the n -by- n covariance matrix $\mathbf{C}(\boldsymbol{\theta})$. Indeed, this requires $\mathcal{O}(n^2)$ memory and $\mathcal{O}(n^3)$ computational steps. Hence, scalable methods that can process larger sample sizes are needed.

Stationary covariance functions, discretized on a rectangular grid, have block Toeplitz structure. This structure can be further extended to a block circulant form [22] and resolved with the Fast Fourier Transform (FFT). The computing cost in this case is $\mathcal{O}(n \log n)$. However, this approach either does not work for data measured at irregularly spaced locations or requires expensive, non-trivial modifications.

During the past two decades, a large amount of research has been devoted to tackling the aforementioned computational challenge of developing scalable methods: for example, covariance tapering [21, 36, 60], likelihood approximations in both the spatial [64] and spectral [19] domains, latent processes such as Gaussian predictive processes [5] and fixed-rank kriging [17], and Gaussian Markov random-field approximations [58, 57, 42, 20]; see [65] for a review. Each of these methods has its strengths and drawbacks. For instance, covariance tapering sometimes performs even worse than assuming independent blocks in the covariance [62]; low-rank approximations have their own limitations [63]; and Markov models depend on the observation locations, requiring irregular locations to be realigned on a much finer grid with missing values [66]. To further improve on these issues, other methods that have been recently developed include the nearest-neighbor Gaussian process models [18], multiresolution Gaussian process models [51], equivalent kriging [40], multi-level restricted Gaussian maximum likelihood estimators [16], and hierarchical low-rank approximations [34]. Bayesian approaches to identify unknown or uncertain parameters could be also applied [55, 56, 49, 46, 49, 52].

In this paper, we propose using the so-called hierarchical (\mathcal{H} -) matrices for approximating dense matrices with numerical complexity and storage $\mathcal{O}(k^\alpha n \log^\alpha n)$, where n is the number of measurements; $k \ll n$ is the rank of the hierarchical matrix, which defines the quality of the approximation; and $\alpha = 1$ or 2 . \mathcal{H} -matrices are suitable for general grids and are also working well for large condition numbers. Previous results [28] show that the \mathcal{H} -matrix technique is very stable when approximating the matrix itself [59, 4, 32, 3, 12], its inverse [3, 9], its Cholesky decomposition [8, 7], and the Schur complement (i.e., the conditional covariance matrix) [28, 43, 44]. Other motivating factors for applying the \mathcal{H} -matrix technique include the following:

1. \mathcal{H} -matrices are more general than other compressed matrix representations (see scheme in Fig. 1);
2. The \mathcal{H} -matrix technique allows us to compute not only the matrix-vector products (e.g.,

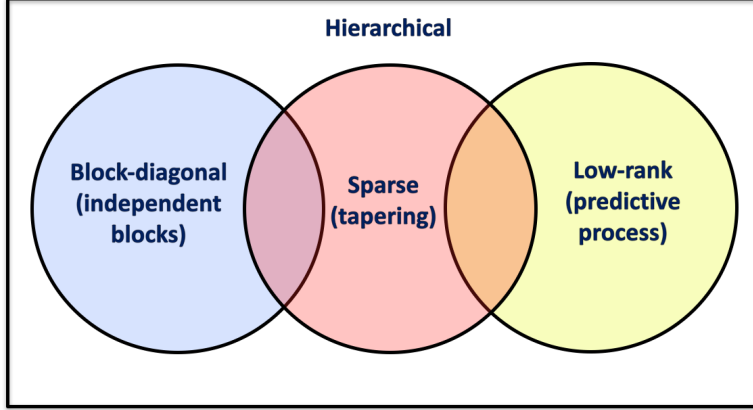


Figure 1: Schema of approximations to the underlying dense covariance matrix (and corresponding methods). Hierarchically low-rank matrices generalize purely structure-based or global schemes with analysis-based locally adaptive schemes.

like fast multipole methods), but also the more general classes of functions, such as $\mathbf{C}(\boldsymbol{\theta})^{-1}$, $\mathbf{C}(\boldsymbol{\theta})^{1/2}$, $|\mathbf{C}(\boldsymbol{\theta})|$, $\exp\{\mathbf{C}(\boldsymbol{\theta})\}$, resolvents, Cholesky decomposition and, many others [28];

3. The \mathcal{H} -matrix technique is well-studied and has solid theory, many examples, and multiple sequential and parallel implementations;
4. The \mathcal{H} -matrix accuracy is controllable by the rank, k . The full rank gives an exact representation;
5. The \mathcal{H} -matrix technique preserves the structure of the matrix after the Cholesky decomposition and the inverse have been computed (see Fig. 2);
6. There are efficient rank-truncation techniques to keep the rank small after the matrix operations; for instance, the Schur complement and matrix inverse can be approximated again in the \mathcal{H} -matrix format.

Figure 2 shows an \mathcal{H} -matrix approximation of the covariance matrix from a discretized ($n = 16,641$) exponential covariance function on the unit square, its Cholesky approximation, and its \mathcal{H} -matrix inverse. The dark (or red) blocks indicate the dense matrices and the grey (green) blocks indicate the rank- k matrices; the number inside each block is its rank. The steps inside the blocks show the decay of the singular values in log scale. The white blocks are empty.

In the last few years, there has been great interest in numerical methods for representing and approximating large covariance matrices in the applied mathematics community [54, 12, 37, 59, 50, 3, 2, 61, 4]. Recently, the maximum likelihood estimator for parameter-fitting Gaussian observations with a Matérn covariance matrix was computed via a framework for unstructured observations in two spatial dimensions, which allowed the evaluation of the log-likelihood and its gradient with computational complexity $\mathcal{O}(n^{3/2})$, where n was the number of observations; the method relied

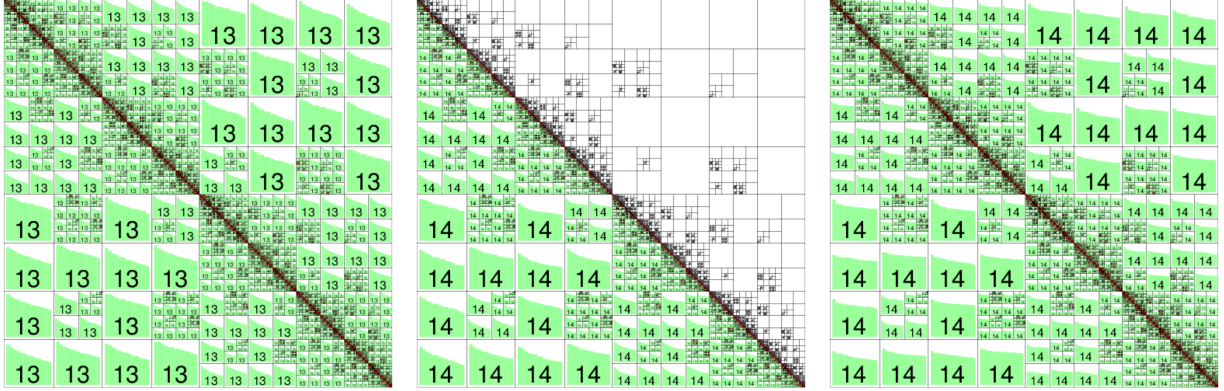


Figure 2: Left: The \mathcal{H} -matrix approximation of an $n \times n$ covariance matrix from a discretized exponential covariance function on the unit square, with $n = 16,641$, unit variance, and length scale of 0.1. The dimensions of the densest (dark) blocks are 32×32 and the maximal rank is $k = 13$. Middle: An example of the corresponding Cholesky factor with maximal rank $k = 14$. Right: The inverse of the exponential covariance matrix (precision matrix) with maximal rank $k = 14$.

on the recursive skeletonization factorization procedure [33, 47]. However, the consequences of the approximation on the maximum likelihood estimator were not studied.

In this paper, we demonstrate that with the computing cost $\mathcal{O}(kn \log n)$ and where $k \ll n$ (usually k is a small integer), we can work with much more general (i.e., not limited to sparse/circulant/structured) covariance matrices.

The rest of this paper is structured as follows. In Section 2, we introduce the \mathcal{H} -matrix technique and review the \mathcal{H} -matrix approximation of Matérn covariance functions. Section 3 contains the hierarchical approximation of the Gaussian likelihood function, the algorithm for parameter estimation, and a study of the theoretical properties and complexity of the approximate log-likelihood [25, 35]. Results from the Monte Carlo simulations of different test cases are reported in Section 4. An application of the hierarchical log-likelihood methodology to soil moisture data is considered in Section 5. We end the paper with a discussion in Section 6. The derivations of the theoretical results are provided in the Appendix A.

2 Hierarchical Approximation of Covariance Matrices

Hierarchical matrices have been described in detail [28, 27, 29, 24, 30, 43]. Applications of the \mathcal{H} -matrix technique to the covariance matrices can be found in [37, 12, 32, 3, 2, 45, 39].

2.1 Hierarchical matrices

In general, covariance matrices are dense and, therefore, require $\mathcal{O}(n^2)$ units of memory for the storage and $\mathcal{O}(n^2)$ FLOPS for the matrix-vector multiplication. In this section, we review the

definition of \mathcal{H} -matrices and show how to approximate covariance matrices using the \mathcal{H} -matrix format. The \mathcal{H} -matrix technique is defined as a hierarchical partitioning of a given matrix into sub-blocks followed by the further approximation of the majority of these sub-block by low-rank matrices (see Fig. 2). To define which sub-blocks can be approximated well by low-rank matrices and which cannot, a so-called admissibility condition is used. After the decomposition of the matrix into sub-blocks has been completed, an important question is how to compute the low-rank approximations. For this purpose, we propose using the Adaptive Cross Approximation (ACA) algorithm [23, 6, 11, 14, 13], which performs the approximations with a linear complexity $\mathcal{O}(n)$.

Remark 2.1 *Errors in the \mathcal{H} -matrix approximation may destroy the symmetry of the symmetric positive definite covariance matrix, causing the symmetric blocks to have different ranks. As a result, the standard algorithms used to compute the Cholesky decomposition may fail. A remedy to this is defining $\mathbf{C} := \frac{1}{2}(\mathbf{C} + \mathbf{C}^\top)$; see also [10].*

Definition 2.1 *We let I be an index set and $T_{I \times I}$ a hierarchical division of the index set product, $I \times I$, into sub-blocks (i.e., we build the so-called block cluster tree). The set of \mathcal{H} -matrices is*

$$\mathcal{H}(T_{I \times I}, k) := \{\mathbf{C} \in \mathbb{R}^{I \times I} \mid \text{rank}(\mathbf{C}|_b) \leq k \text{ for all admissible blocks } b \text{ of } T_{I \times I}\},$$

where k is the maximum rank. Here, $\mathbf{C}|_b = (c_{ij})_{(i,j) \in b}$ denotes the matrix block of $\mathbf{C} = (c_{ij})_{i,j \in I}$ corresponding to $b \in T_{I \times I}$.

Blocks that satisfy the admissibility condition can be approximated by low-rank matrices; see [27]. An \mathcal{H} -matrix approximation of \mathbf{C} is denoted by $\tilde{\mathbf{C}}$. The storage requirement of $\tilde{\mathbf{C}}$ and the matrix vector multiplication cost $\mathcal{O}(kn \log n)$, the matrix-matrix addition costs $\mathcal{O}(k^2 n \log n)$, and matrix-matrix product, and the matrix inverse cost $\mathcal{O}(k^2 n \log^2 n)$; see [27].

Remark 2.2 *There are two different \mathcal{H} -matrix approximation strategies. 1) The fixed rank strategy, i.e., each sub-block has maximal rank k . We cannot determine the accuracy in each sub-block using this strategy; it could be very high or it could be very low. In this case we write $\mathcal{H}(T_{I \times I}; k)$, or $\tilde{\mathcal{L}}(\boldsymbol{\theta}; k)$. 2) The adaptive rank strategy, i.e., where absolute accuracy (in the spectral norm) for each sub-block is ε or better (smaller). We can only approximately estimate the total computing cost and storage using this strategy. In this case, we write $\mathcal{H}(T_{I \times I}; \varepsilon)$ and $\tilde{\mathcal{L}}(\boldsymbol{\theta}; \varepsilon)$.*

The fixed rank strategy is useful for a priori evaluations of the computational resources and storage memory. The adaptive rank strategy is preferable for practical approximations and is useful when the accuracy in each sub-block is crucial.

2.2 Matérn covariance functions

Among the many covariance models available, the Matérn family [48] has gained widespread interest in recent years. The Matérn form of spatial correlations was introduced into statistics as a flexible parametric class, with one parameter determining the smoothness of the underlying spatial random field [31]. The varied history of this family of models can be found in [26].

The Matérn covariance depends only on the distance $h := \|\mathbf{s} - \mathbf{s}'\|$, where \mathbf{s} and \mathbf{s}' are any two spatial locations. The Matérn class of covariance functions is defined as

$$C(h; \boldsymbol{\theta}) = \frac{\sigma^2}{2^{\nu-1}\Gamma(\nu)} \left(\frac{h}{\ell}\right)^\nu K_\nu\left(\frac{h}{\ell}\right), \quad (2)$$

with $\boldsymbol{\theta} = (\sigma^2, \ell, \nu)^\top$; where σ^2 is the variance; $\nu > 0$ controls the smoothness of the random field, with larger values of ν corresponding to smoother fields; and $\ell > 0$ is a spatial range parameter that measures how quickly the correlation of the random field decays with distance, with larger ℓ corresponding to a faster decay (keeping ν fixed) [32, 37]. Here K_ν denotes the modified Bessel function of the second kind of order ν . When $\nu = 1/2$, the Matérn covariance function reduces to the exponential covariance model and describes a rough field. The value $\nu = \infty$ corresponds to a Gaussian covariance model that describes a very smooth, infinitely differentiable field. Random fields with a Matérn covariance function are $\lfloor \nu - 1 \rfloor$ times mean square differentiable.

2.3 Matérn covariance matrix approximation

By definition, covariance matrices are symmetric, positive semi-definite, and have positive real eigenvalues. The decay of the eigenvalues (that is, the \mathcal{H} -matrix rank- k approximation) depends on the type of the covariance matrix and its smoothness, covariance length, computational geometry, and dimensionality. In this section, we perform numerical experiments with \mathcal{H} -matrix approximations.

To underline the fact that \mathcal{H} -matrix representations apply to irregular meshes, we use irregularly spaced locations in the unit square:

$$\frac{1}{\sqrt{n}} (i - 0.5 + X_{ij}, j - 0.5 + Y_{ij}), \quad \text{for } i, j \in \{1, 2, \dots, \sqrt{n}\}, \quad (3)$$

where X_{ij}, Y_{ij} are i.i.d. uniform on $(-0.4, 0.4)$ for a total of n observations; see [66]. The observations are ordered lexicographically by the ordered pair (i, j) .

All of the numerical experiments herein are performed on a Dell workstation with 20 processors (40 cores) and total 128 GB RAM. The parallel \mathcal{H} -matrix library, HLIBPro [41], was used to build the Matérn covariance matrix, compute the Cholesky factorization, solve a linear system, calculate the determinant and the quadratic form. HLIBPro is fast and efficient; see the theoretical parallel scalability in Table 1. Here $|V(T)|$ denotes the number of vertices, $|L(T)|$ the number of leaves in the block-cluster tree $T = T_{I \times I}$, and n_{min} the size of a block when we stop further division into sub-blocks (see Section 2.1). Usually $n_{min} = 32$ or 64 , since a very deep hierarchy slows down computations.

Table 2 shows the \mathcal{H} -matrix approximation errors for $\log |\tilde{\mathbf{C}}|$, $\tilde{\mathbf{C}}$ and the inverse $(\tilde{\mathbf{L}}\tilde{\mathbf{L}}^\top)^{-1}$, where $\tilde{\mathbf{L}}$ is the Cholesky factor. The errors are computed in the Frobenius and spectral norms, where \mathbf{C} is the exact Matérn covariance matrix with $\nu = 0.5$ and $\sigma^2 = 1$. The local accuracy in each sub-block is ε . The number of locations is $n = 16,641$. The last column demonstrates the total compression ratio, c.r., which is equal to $1 - \text{size}(\tilde{\mathbf{C}})/\text{size}(\mathbf{C})$. The exact values are $\log |\mathbf{C}| = 2.63$ for $\ell = 0.0334$

Table 1: Scalability of the main linear operations in HLIB and HLIBPro on p processors.

Operation	Sequential Complexity	Parallel Complexity [41] (Shared Memory)
build $\tilde{\mathbf{C}}$	$\mathcal{O}(n \log n)$	$\frac{\mathcal{O}(n \log n)}{p} + \mathcal{O}(V(T) \setminus L(T))$
store $\tilde{\mathbf{C}}$	$\mathcal{O}(kn \log n)$	$\mathcal{O}(kn \log n)$
$\tilde{\mathbf{C}} \cdot \mathbf{z}$	$\mathcal{O}(kn \log n)$	$\frac{\mathcal{O}(kn \log n)}{p} + \frac{n}{\sqrt{p}}$
$\tilde{\mathbf{C}}^{-1}$	$\mathcal{O}(k^2 n \log^2 n)$	$\frac{\mathcal{O}(n \log n)}{p} + \mathcal{O}(nn_{min}^2)$, $1 \leq n_{min} \leq 128$
\mathcal{H} -Cholesky $\tilde{\mathbf{L}}$	$\mathcal{O}(k^2 n \log^2 n)$	$\frac{\mathcal{O}(n \log n)}{p} + \mathcal{O}(\frac{k^2 n \log^2 n}{n^{1/d}})$
$ \tilde{\mathbf{C}} $	$\mathcal{O}(k^2 n \log^2 n)$	$\frac{\mathcal{O}(n \log n)}{p} + \mathcal{O}(\frac{k^2 n \log^2 n}{n^{1/d}})$, $d = 1, 2, 3$

Table 2: The parallel \mathcal{H} -matrix accuracy and compression rates (c.r.). Number of computing cores is 40. Accuracy in each sub-block is ε ; $n = 16,641$, $\tilde{\mathbf{C}}$ is a Matérn covariance with $\nu = 0.5$ and $\sigma^2 = 1$. The spatial domain is the unit square with locations irregularly spaced as in (3).

ε	$ \log \mathbf{C} - \log \tilde{\mathbf{C}} $	$ \frac{\log \mathbf{C} - \log \tilde{\mathbf{C}} }{\log \tilde{\mathbf{C}} } $	$\ \mathbf{C} - \tilde{\mathbf{C}}\ _F$	$\frac{\ \mathbf{C} - \tilde{\mathbf{C}}\ _2}{\ \tilde{\mathbf{C}}\ _2}$	$\ \mathbf{I} - (\tilde{\mathbf{L}}\tilde{\mathbf{L}}^\top)^{-1}\tilde{\mathbf{C}}\ _2$	c.r. (%)
$\ell = 0.0334$						
10^{-1}	$3.2 \cdot 10^{-4}$	$1.2 \cdot 10^{-4}$	$7.0 \cdot 10^{-3}$	$7.6 \cdot 10^{-3}$	2.9	91.8
10^{-2}	$1.6 \cdot 10^{-6}$	$6.0 \cdot 10^{-7}$	$1.0 \cdot 10^{-3}$	$6.7 \cdot 10^{-4}$	$9.9 \cdot 10^{-2}$	91.6
10^{-4}	$1.8 \cdot 10^{-9}$	$7.0 \cdot 10^{-10}$	$1.0 \cdot 10^{-5}$	$7.3 \cdot 10^{-6}$	$2.0 \cdot 10^{-3}$	89.8
10^{-8}	$4.7 \cdot 10^{-13}$	$1.8 \cdot 10^{-13}$	$1.3 \cdot 10^{-9}$	$6 \cdot 10^{-10}$	$2.1 \cdot 10^{-7}$	97.3
$\ell = 0.2337$						
10^{-4}	$9.8 \cdot 10^{-5}$	$1.5 \cdot 10^{-5}$	$8.1 \cdot 10^{-5}$	$1.4 \cdot 10^{-5}$	$2.5 \cdot 10^{-1}$	91.5
10^{-8}	$1.5 \cdot 10^{-9}$	$2.3 \cdot 10^{-10}$	$1.1 \cdot 10^{-8}$	$1.5 \cdot 10^{-9}$	$4 \cdot 10^{-5}$	88.7

and $\log |\mathbf{C}| = 6.36$ for $\ell = 0.2337$. The uniformly distributed mesh points are taken in the unit square and perturbed as in (3).

3 Hierarchical Approximation of Gaussian Likelihood

3.1 Parameter estimation

We use the \mathcal{H} -matrix technique to approximate the Gaussian likelihood function. The \mathcal{H} -matrix approximation of the exact log-likelihood $\mathcal{L}(\boldsymbol{\theta})$ defined in (1) is defined by $\tilde{\mathcal{L}}(\boldsymbol{\theta}; k)$:

$$\tilde{\mathcal{L}}(\boldsymbol{\theta}; k) = -\frac{n}{2} \log(2\pi) - \sum_{i=1}^n \log\{\tilde{\mathbf{L}}_{ii}(\boldsymbol{\theta}; k)\} - \frac{1}{2} \mathbf{v}(\boldsymbol{\theta})^\top \mathbf{v}(\boldsymbol{\theta}), \quad (4)$$

where $\tilde{\mathbf{L}}(\boldsymbol{\theta}; k)$ is the rank- k \mathcal{H} -matrix approximation of the Cholesky factor $\mathbf{L}(\boldsymbol{\theta})$ in $\mathbf{C}(\boldsymbol{\theta}) = \mathbf{L}(\boldsymbol{\theta})\mathbf{L}(\boldsymbol{\theta})^\top$, and $\mathbf{v}(\boldsymbol{\theta})$ is the solution of the linear system $\tilde{\mathbf{L}}(\boldsymbol{\theta}; k)\mathbf{v}(\boldsymbol{\theta}) = \mathbf{Z}$.

The \mathcal{H} -matrix approximation $\tilde{\mathcal{L}}(\boldsymbol{\theta}; k)$ in (4) is the fixed rank strategy, i.e., each sub-block in the covariance matrix has a rank equal to k or smaller (and the accuracy in each sub-block is unknown).

To maximize $\tilde{\mathcal{L}}(\boldsymbol{\theta}; k)$ in (4), we use Brent's method [15, 53], also known as Brent-Dekker. The Brent-Dekker algorithm first uses the fast-converging secant method or inverse quadratic interpolation to maximize $\tilde{\mathcal{L}}(\boldsymbol{\theta}; \cdot)$. If those do not work, then it returns to the more robust bisection method. We note that the maximization of the log-likelihood function is an ill-posed problem, since even very small perturbations in the covariance matrix $\mathbf{C}(\boldsymbol{\theta})$ may result in huge perturbations in the log-determinant and the log-likelihood. An alternative to $\mathbf{C}(\boldsymbol{\theta}) = \mathbf{L}(\boldsymbol{\theta})\mathbf{L}(\boldsymbol{\theta})^\top$ is the $\mathbf{L}(\boldsymbol{\theta})\mathbf{D}(\boldsymbol{\theta})\mathbf{L}^\top(\boldsymbol{\theta})$ decomposition, which is more stable since it can avoid extracting square roots of diagonal elements. In our numerical experiments below we use $\mathbf{L}(\boldsymbol{\theta})\mathbf{D}(\boldsymbol{\theta})\mathbf{L}^\top$ factorization.

3.2 Computational complexity and accuracy

Theorem 1 (*Computational complexity for computing the hierarchical log-likelihood*)

We let $\mathbf{C}(\boldsymbol{\theta}) \in \mathbb{R}^{n \times n}$ be approximated by an \mathcal{H} -matrix $\tilde{\mathbf{C}}(\boldsymbol{\theta}; k)$ with a maximal rank k . Then, the cost of computing the log-likelihood function $\tilde{\mathcal{L}}(\boldsymbol{\theta}; k)$ is $\mathcal{O}(k^2 n \log^2 n)$ and the cost of computing the MLE in $\#\mathcal{I}$ iterations is $\mathcal{O}(\#\mathcal{I} \cdot k^2 n \log^2 n)$.

The proof follows from the \mathcal{H} -matrix cost estimates. The Cholesky decomposition costs $\mathcal{O}(k^2 n \log^2 n)$. The solution of the linear system $\tilde{\mathbf{L}}(\boldsymbol{\theta}; k)\mathbf{v}(\boldsymbol{\theta}) = \mathbf{Z}$ costs $\mathcal{O}(k^2 n \log^2 n)$. The log-determinant $\log |\tilde{\mathbf{C}}(\boldsymbol{\theta}; k)| = 2 \sum_{i=1}^n \log \{\tilde{\mathbf{L}}_{ii}(\boldsymbol{\theta}; k)\}$ is available for free.

Once we observe a realization \mathbf{z} of the random vector \mathbf{Z} , we can quantify the accuracy of the \mathcal{H} -matrix approximation of the log-likelihood function. Our main theoretical result is formulated below in Theorem 2.

Theorem 2 (*Accuracy of the log-likelihood*)

We let $\tilde{\mathbf{C}}(\boldsymbol{\theta}; k)$ be an \mathcal{H} -matrix approximation of the matrix $\mathbf{C}(\boldsymbol{\theta}) \in \mathbb{R}^{n \times n}$ and \mathbf{z} a data vector. We assume $\|\mathbf{z}\| \leq c_0$ and $\|\mathbf{C}^{-1}\| \leq c_1$, where $c_0, c_1 > 0$ are some constants, and the spectral radius $\rho(\tilde{\mathbf{C}}(\boldsymbol{\theta})^{-1}\mathbf{C}(\boldsymbol{\theta}) - \mathbf{I}) < \varepsilon < 1$. Then the following statements are hold

$$\begin{aligned} |\log |\tilde{\mathbf{C}}(\boldsymbol{\theta}; k)| - \log |\mathbf{C}(\boldsymbol{\theta})|| &\leq -n \log(1 - \varepsilon) \approx n\varepsilon \quad \text{for small } \varepsilon, \\ |\tilde{\mathcal{L}}(\boldsymbol{\theta}; k) - \mathcal{L}(\boldsymbol{\theta})| &\leq \frac{1}{2} \cdot n\varepsilon + \frac{1}{2} c_0^2 \cdot c_1 \cdot \varepsilon. \end{aligned}$$

Proof: See in the Appendix A.

It has been observed that the bound n in the inequalities above is pessimistic and is hardly observed in numerical simulations [4]. Though Theorem 2 is shown for the fixed rank arithmetics, it also holds for the adaptive rank arithmetics with $\tilde{\mathbf{C}}(\boldsymbol{\theta}; \varepsilon)$.

4 Monte Carlo Simulations

We performed numerical experiments with simulated data to recover the true values of the parameters of the Matérn covariance matrix, known to be $(\ell^*, \nu^*, \sigma^*) = (0.0864, 0.5, 1.0)$. To build various data sets with $n \in \{128, 64, \dots, 4, 2\} \times 1000$ locations, we took a fine mesh with $n_0 = 2 \cdot 10^6$ locations and randomly sampled n points from it. If locations are very close to each other, then the

covariance matrix could be singular or it will be difficult to compute the Cholesky factorization. To avoid this problem, we took these $2 \cdot 10^6$ locations from the daily moisture example, which is described below in Sect. 5. Then we generated random data $\mathbf{Z} = \tilde{\mathbf{L}} \cdot \boldsymbol{\xi}$, where $\boldsymbol{\xi} \in \mathbb{R}^{n_0}$ is a normal vector with zero mean and unit variance, and $\tilde{\mathbf{C}} = \tilde{\mathbf{L}} \cdot \tilde{\mathbf{L}}^\top$. We did it only once. After that we ran our optimization algorithm and tried to identify (recover) the “unknown” parameters $(\ell^*, \nu^*, \sigma^*)$. The boxplots for each parameter over 50 replicates are illustrated in Figure 3.

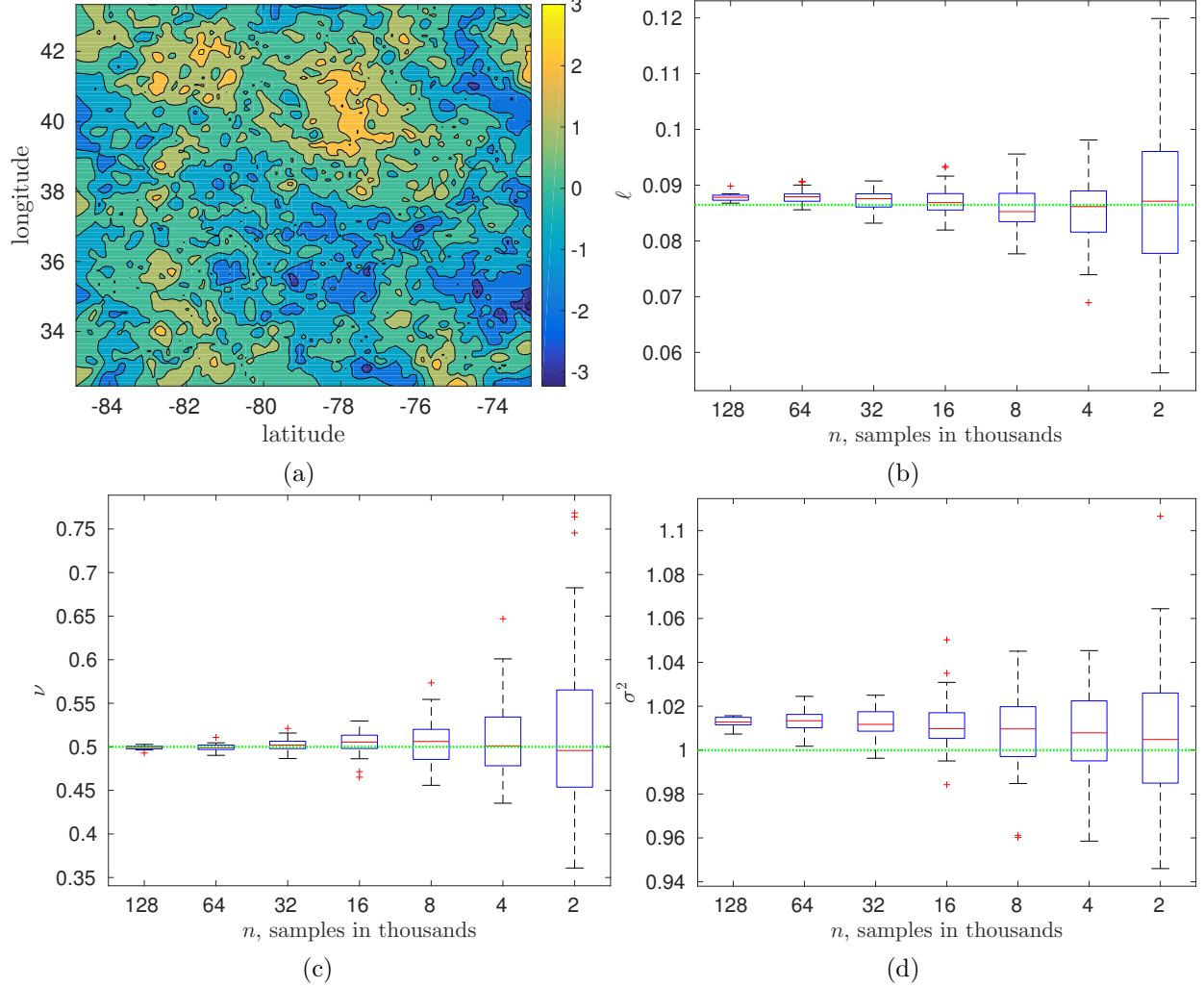


Figure 3: Simulated data with known parameters $(\ell^*, \nu^*, \sigma^*) = (0.0864, 0.5, 1.0)$. (a) One realization of a random field, generated in MATLAB from simulated data at 2000 locations. (b) Boxplots for ℓ , (c) ν , and (d) σ^2 for $n = 1,000 \times \{128, 64, 32, 16, 8, 4, 2\}$. Boxplots are obtained from 50 replicates. All of the estimates are obtained by using the \mathcal{H} -matrix sub-block accuracy $\varepsilon = 10^{-6}$.

For the sake of reproducibility of all numerical experiments below, we stored all our generated data sets.

Remark 4.1 *We did not simulate the vector \mathbf{Z} for each of the 50 replicates. Instead, we generated only once a normal vector $\boldsymbol{\xi}$ of size $n_0 = 2 \cdot 10^6$ with zero mean and unit variance and computed*

$\mathbf{Z} = \tilde{\mathbf{L}} \cdot \boldsymbol{\xi}$. We created data sets by sampling 50 times for each dimension $n \in \{2, 4, \dots, 128\} \times 1000$ from \mathbf{Z} . As a result we obtained 50 data sets of size 2,000; 50 data sets of size 4,000, and so on. In this way we tried to mimic the experiment done with the daily moisture data, where we have only one large vector of observations. We note that the way how we create data sets may influence the behavior of boxplots and medians.

One realization of a Gaussian random field, which has a Matérn covariance function with parameters $(\ell^*, \nu^*, \sigma^*) = (0.0864, 0.5, 1.0)$, is presented in Fig. 3a. To build this realization we used the MATLAB function `scatteredInterpolant(.)` for interpolation and `counturf(.)` for visualization. We assumed that measurements in 2,000 locations are known. This simulation study (Fig. 3) shows that the suggested method is able to identify the unknown parameters of a Matérn covariance function on an irregular grid. A small bias, around 1%, on Fig. 3d, for the variance σ^2 can be explained by the simulation design that was employed.

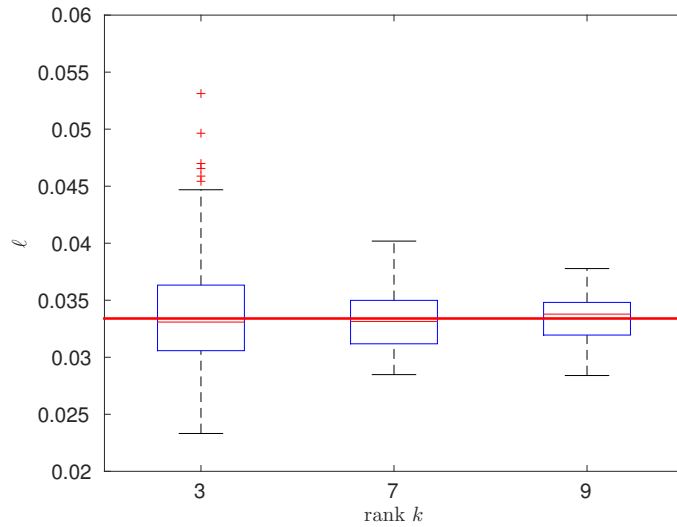


Figure 4: Simulated data, $n = 16,641$. Boxplots of ℓ vs. different \mathcal{H} -matrix ranks $k = \{3, 7, 9\}$; $\nu = 0.5$, $\ell = 0.0334$, $\sigma^2 = 1$.

In Fig. 4 we present three boxplots for the \mathcal{H} -matrix ranks $k = \{3, 7, 9\}$. The true value, denoted by a solid line, is $\ell = 0.0334$. When increasing the \mathcal{H} -matrix accuracy (rank k), the boxplot for ℓ contracts. Since the rank k appears quadratically in the complexity estimates and linearly in the storage estimate, one replicate for rank $k = 9$ requires $3^2 = 9$ times more FLOPs than a replicate for rank $k = 3$, and three times more storage memory. The reason for the shrinking boxplots is that the \mathcal{H} -matrix approximation error also decreases with increasing k . From these boxplots, we can find the optimal rank k , i.e., the computational resources and memory storage needed to reach a certain level of precision.

5 Application to Soil Moisture Data

5.1 Problem and data description

In climate and weather studies, numerical models play an important role in improving our knowledge of the characteristics of the climate system, and the causes behind climate variations. These numerical models describe the evolution of many variables, such as temperature, wind speed, precipitation, humidity, and pressure, by solving a set of equations. The process is usually very complicated, involving physical parameterization, initial condition configurations, numerical integration, and data output schemes. In this section, we use the proposed \mathcal{H} -matrix methodology to investigate the spatial variability of soil moisture data, as generated by numerical models. Soil moisture is a key factor in evaluating the state of the hydrological process and has a broad range of applications in weather forecasting, crop yield prediction, and early warnings of flood and drought. It has been shown that a better characterization of soil moisture can significantly improve weather forecasting. However, numerical models often generate very large datasets due to the high spatial resolutions of the measured data, which makes the computation of the widely used Gaussian process models infeasible. Consequently, the whole region of interest must be divided into blocks of smaller size in order to fit the Gaussian process models independently to each block; alternatively, the size of the dataset must be reduced by averaging to a lower spatial resolution. Compared to fitting a consistent Gaussian process model to the entire region, it is unclear how much statistical efficiency is lost by such an approximation. Since our proposed \mathcal{H} -matrix technique can handle large covariance matrix computations, and the parallel implementation of the algorithm significantly reduces the computational time, we are able to fit Gaussian process models to a set of large subsamples in a given spatial region. Therefore, next we explore the effect of sample size on the statistical efficiency.

We consider high-resolution soil moisture data from January 1, 2014, measured in the topsoil layer of the Mississippi River basin, U.S.A. The spatial resolution is 0.0083 degrees, and the distance of one-degree difference in this region is approximately 87.5 km. The grid consists of $1830 \times 1329 = 2,432,070$ locations, with missing values. Therefore, the available spatial data are not on a regular grid. We use the same model for the mean process as in Huang and Sun (2017), and fit a zero-mean Gaussian process model with a Matérn covariance function to the residuals; see Huang and Sun (2017) for more details on the data description and exploratory data analysis.

5.2 Numerical tests with soil moisture data

To understand the uncertainty of the parameter estimation, we randomly pick up: 100 data sets of size $n = 2,000$; 100 data sets of size 4,000;... and 100 data sets of size 128,000 from 2,432,070 available points. The distributions of the 100 parameter estimates for each n are summarized in Fig. 5. In each iteration we solve a three-dimensional optimization problem and identify all three parameters simultaneously. The behavior and accuracy of the boxplots depend on such factors as the hierarchical matrix rank, the maximum number of iterations to achieve a certain threshold, the

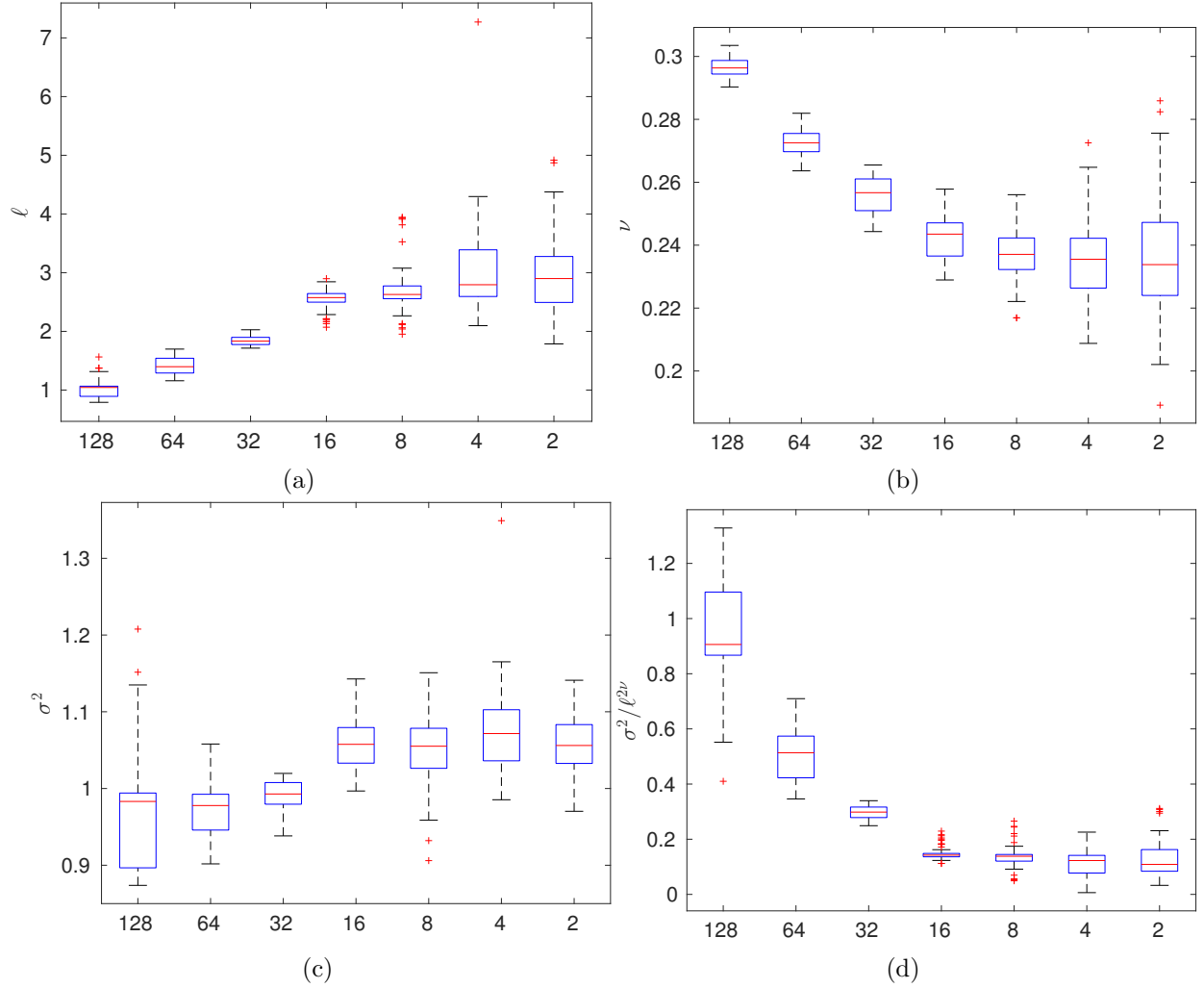


Figure 5: Soil moisture data example. Boxplots for the 100 estimates of ℓ (a), ν (b), σ^2 (c), and $\frac{\sigma^2}{\ell^{2\nu}}$ (d) for $n = \{128,000, \dots, 2,000\}$. All of the estimates are obtained using the \mathcal{H} -matrix sub-block accuracy, $\varepsilon = 10^{-6}$.

threshold (or residual) itself, the initial guess, the step size in each parameter in the maximization algorithm, and the maximization algorithm. For $n = \{2,000, \dots, 16,000\}$, the medians are similar, while the sizes of the boxplots are decreasing. For $n = \{32,000, \dots, 128,000\}$, the medians are different. A possible explanation could be that on a sufficiently fine mesh, the daily moisture data have some other fine-scale properties. We refer to work [1], where the authors decomposed the initial large domain into 16 subdomains and estimated all three parameters in each subdomain. One can see, that the variation between subdomains is quite high. There are regions with high variability (variance) and with low variability. A mesh with 128,000 nodes covers the domain much more uniformly than a mesh with just 2,000 and can recover much more fine details than a mesh with 2,000 nodes. These fine details may be invisible on coarser meshes, but become visible on finer meshes. Another explanation could be that the Matérn covariance function is not suitable for

describing these daily moisture data. Another model or a mixture of different Matérn functions may be needed. Finally, we note that the 3D-solution is not unique — there are many triplets $(\hat{\ell}, \hat{\sigma}, \hat{\theta})$ which satisfy the prescribed residual 10^{-6} and reducing the residual will require much more expensive iterations.

Remark 5.1 *We also emphasize that only one vector \mathbf{Z} is available and we sampled all our data sets only from this vector. In the case when many vectors \mathbf{Z} are available (e.g., daily observations during multiple days) the behavior of boxplots could be different.*

In Fig. 6 we present one realization generated from the fitted model, where the Matérn covariance function has parameters $(\hat{\ell}, \hat{\nu}, \hat{\sigma}^2) = (1.5, 0.28, 1.45)$. To visualize this realization, we used the MATLAB functions *scatteredInterpolant*(\cdot) for the interpolation and *contourf*(\cdot) for the visualization. We used 2,000 (left) and 40,000 (right) locations.

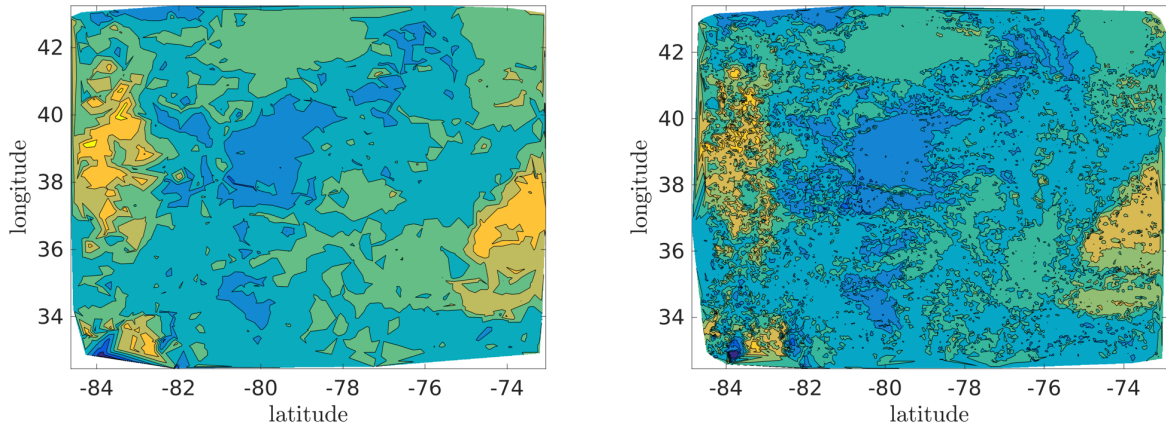


Figure 6: One realization of random field, generated in MATLAB from soil moisture data $(\ell^*, \nu^*, \sigma^*) = (1.5, 0.28, 1.45)$ with 2,000 (left) and 40,000 (right) locations.

Next, we investigated the impact of the sample size n on the likelihood optimization. For simplicity, we chose one dataset for each n and plotted $\tilde{\mathcal{L}}/n$ as a function of ℓ and ν , respectively, while keeping the other parameters fixed. We found that the sample size n does have an impact on optimization. Figure 7 (left) shows the dependence of the negative log-likelihood functions, divided by n , on ℓ (on the left) and on ν (on the right). Although the minima appear within a relatively small interval in all of the cases, it is clear that the resulting log-likelihoods are more difficult to optimize for $n = 2,000$ and $n = 4,000$.

We now present an example to show the \mathcal{H} -matrix inversion error $\|\mathbf{I} - (\tilde{\mathbf{L}}\tilde{\mathbf{L}}^\top)^{-1}\tilde{\mathbf{C}}\|_2$, for $n = 2,000$ locations taken from the soil moisture data example in Section 5. For this data set, the estimated parameters are $(\hat{\ell}, \hat{\nu}, \hat{\sigma}^2)$. Figure 8 shows the dependence of the \mathcal{H} -matrix inversion error $\|\mathbf{I} - (\tilde{\mathbf{L}}\tilde{\mathbf{L}}^\top)^{-1}\tilde{\mathbf{C}}\|_2$ of the Matérn covariance matrix (as well as the precision matrix $\tilde{\mathbf{C}}^{-1}$) on the parameters ℓ and ν , when the other two parameters are fixed. The \mathcal{H} -matrix sub-block accuracy is $\varepsilon = \{10^{-4}, 10^{-6}\}$, i.e., adaptive-rank. The sizes of the corresponding \mathcal{H} -matrices reminded almost

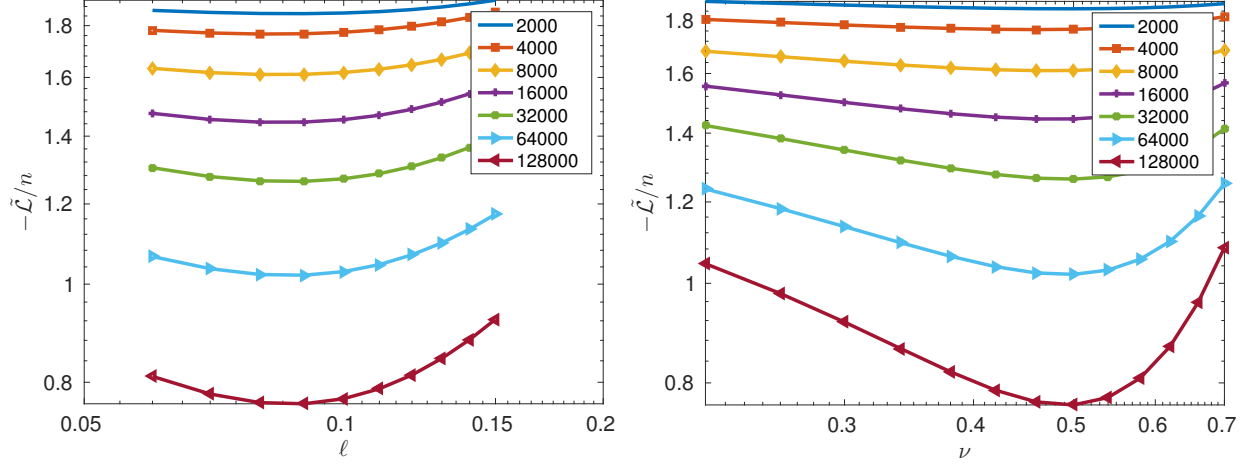


Figure 7: Dependence of the negative log-likelihood function, divided by n , on $n = \{2,000, \dots, 128,000\}$ and on the parameters ℓ (left) and ν (right), in log-log scale for the soil moisture data example.

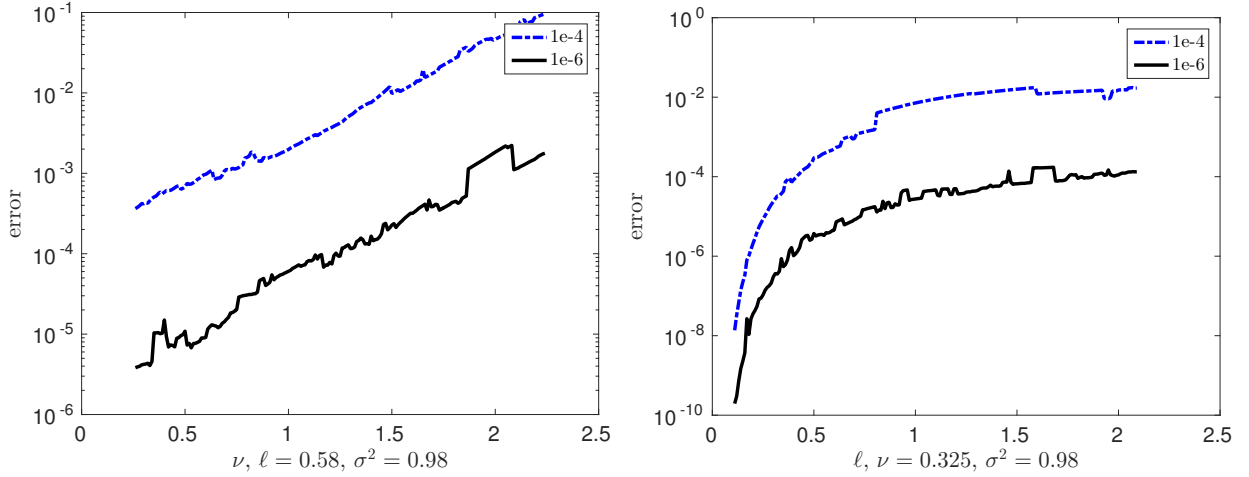


Figure 8: Soil moisture data example with $n = 2,000$ locations. Dependence of the \mathcal{H} -matrix inversion error $\|\mathbf{I} - (\tilde{\mathbf{L}}\tilde{\mathbf{L}}^\top)^{-1}\tilde{\mathbf{C}}\|_2$ on (left) the smoothness parameter ν ($\hat{\ell} = 0.58$, $\hat{\sigma}^2 = 0.98$ fixed) and (right) the covariance length ℓ ($\hat{\nu} = 0.325$, $\hat{\sigma}^2 = 0.98$ fixed). The \mathcal{H} -matrix accuracy in each sub-block is $\varepsilon = \{10^{-4}, 10^{-6}\}$.

the same, they varied from 4.6 MB to 5.4 MB for $\varepsilon = 10^{-4}$, and from 6.0 MB to 6.6 MB for $\varepsilon = 10^{-6}$, where $\nu \in (0.32, 2.25)$ and $\ell \in (0.1, 2.3)$.

Figure 9 shows one example of the approximated covariance matrix of the soil moisture data when $n = 8,000$ with $\hat{\nu} = 0.325$, $\hat{\ell} = 0.64$, and $\hat{\sigma}^2 = 0.98$ in the Matérn covariance function. We used adaptive ranks in this approximation.

We fixed the accuracy (in the spectral norm) inside of each sub-block; for the matrix itself we chose $\varepsilon = 10^{-3}$ and for the Cholesky factor, $\varepsilon = 10^{-8}$. Since the matrix sub-blocks were different sizes, and at various distances from the diagonal (singularity), we observed different ranks inside

Table 3: Computing time and storage cost for parallel \mathcal{H} -matrix approximation; number of cores is 40, $\hat{\nu} = 0.325$, $\hat{\ell} = 0.64$, $\hat{\sigma}^2 = 0.98$. \mathcal{H} -matrix accuracy in each sub-block for both $\tilde{\mathbf{C}}$ and $\tilde{\mathbf{L}}$ is 10^{-5} .

n	$\tilde{\mathbf{C}}$			$\tilde{\mathbf{L}}\tilde{\mathbf{L}}^\top$		
	time sec.	size MB	kB/dof	time sec.	size MB	$\ \mathbf{I} - (\tilde{\mathbf{L}}\tilde{\mathbf{L}}^\top)^{-1}\tilde{\mathbf{C}}\ _2$
32,000	3.2	160	5.1	2.3	172.7	$2.5 \cdot 10^{-3}$
64,000	5.3	353	5.6	5.1	392.5	$5.4 \cdot 10^{-3}$
128,000	13.2	770	6.2	13.7	881.2	$1.0 \cdot 10^{-2}$
256,000	32.5	1600	6.6	35.5	1890	$1.7 \cdot 10^{-2}$
512,000	52.0	3410	7.0	77.4	4150	$3.4 \cdot 10^{-2}$
1,000,000	103	7070	7.4	187	8830	$6.6 \cdot 10^{-2}$
2,000,000	227	14720	7.7	471	18970	$1.3 \cdot 10^{-1}$

one on σ^2 , when all other parameters remain fixed. From these figures, we can see that it is hard for the minimization algorithm to find the minima. The solid black line is almost horizontal, and many points may satisfy the residual. One possible remedy is to use a very small residual (we used 10^{-6}), but this will require many expensive iterations. We also see that the solution may depend on the initial conditions in the minimization algorithm. If the initial conditions are very far from the global minima, then the maximal number of iterations (which is also a parameter in the minimization algorithm) may not be sufficient to achieve these global maxima.

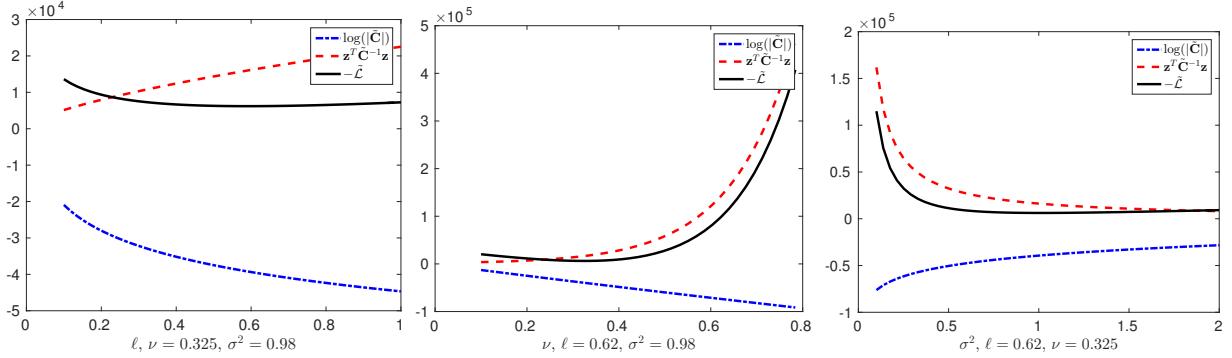


Figure 10: Moisture example with $n = 32,000$ locations. Dependence of log-likelihood, log-determinant and the quadratic form on parameters. Computations are performed with \mathcal{H} -matrix rank $k = 11$.

5.3 Reproducibility of numerical results

To reproduce the presented numerical simulations, the first step is downloading the HLIB (www.hlib.org) or HLIBPro (www.hlibpro.com) libraries. Both are free for academic purposes. HLIB is a sequential, open-source C-code library, which is relatively easy to use and understand. HLIBPro is the highly tuned parallel version of HLIB, where only the header and object files are accessible.

After signing the \mathcal{H} -matrix (HLIB or HLIBPro) license, downloading, and installing the libraries, our modules for approximating covariance matrices and computing log-likelihoods, and the soil moisture data can be downloaded from <https://github.com/litvinen/HLIBCov.git>.

HLIB requires not only the set of locations, but also the corresponding triangulation of the computing domains [43, 38]. The vertices of the triangles should be used as the location points. To construct a triangulation, we recommend employing the routines in MATLAB, R, or any other third-party software. HLIBPro does not require triangulation; only the coordinates of the locations are needed.

6 Conclusion and Discussion

We have developed a tool relying on novel constructs from linear algebra that can improve the quality of statistical forecasts, by making it possible to work with large datasets of measurements observed on unstructured grids, in particular a new method of estimating the unknown parameters of a covariance model. The statistical model includes the class of Matérn covariance matrices with three unknown parameters, ℓ , ν , and σ^2 . We applied the \mathcal{H} -matrix technique in approximating multivariate Gaussian log-likelihood functions and Matérn covariance matrices. The \mathcal{H} -matrix technique allowed us to drastically reduce the required memory (Table 2) and computing time (Table 3). Within the \mathcal{H} -matrix approximation, we can increase the spatial resolution, take more measurements into account, and consider larger regions with larger data sets. \mathcal{H} -matrices require neither axes-parallel grids nor homogeneity of the covariance function.

From the \mathcal{H} -matrix approximation of the log-likelihood, we computed the \mathcal{H} -Cholesky factorization, the log-determinant, and a quadratic form, $\mathbf{Z}^\top \mathbf{C}^{-1} \mathbf{Z}$ (Table 2). We demonstrated the computing time, storage requirements, relative errors, and convergence of the \mathcal{H} -matrix technique (Table 3, Fig. 8).

We reduced the cost of computing the log-likelihood function dramatically, from cubic to almost linear (see Table 3), by employing the \mathcal{H} -matrix approximations, without significantly changing the log-likelihood, even with a small rank k . We considered both a simulated example, where we identified the known parameters, and a large, real data (soil moisture) example, where the parameters were unknown. We were able to calculate the maximum of the log-likelihood and the maximum likelihood estimator (MLE) for both examples. We were also able to compute the MLE when all of the parameters ℓ , ν , and σ^2 , were simultaneously unknown. We researched the contributions of the \mathcal{H} -matrix approximation error and the statistical error (see Fig. 4) to the total error. We found a balance between the \mathcal{H} -matrix approximation error and the statistical error; Fig. 4. Boxplots for the estimates of ℓ , ν , and σ^2 for $n = \{128,000, \dots, 2,000\}$ are shown in Figure 5.

We found how the log-likelihood function and MLE depend on the number of locations (Fig. 7), which we varied from 2,000 to 128,000. We demonstrated that the \mathcal{H} -matrix approximation errors are stable with respect to the Matérn parameters ℓ , ν , and σ^2 . Since the \mathcal{H} -matrix approximation is much cheaper to store than the original matrix, a much larger number of locations can be considered. With the parallel \mathcal{H} -matrix library HLIBPro, we were able to compute the log-likelihood

function for 2,000,000 locations just in a few minutes on a desktop machine (Fig. 3).

Acknowledgment The research reported in this publication was supported by funding from King Abdullah University of Science and Technology (KAUST). Additionally, we would like to express our special thanks of gratitude to Ronald Kriemann (for the HLIBPro software library) as well as to Lars Grasedyck and Steffen Boerm for the HLIB software library.

References

- [1] S. Abdulah, H. Ltaief, Y. Sun, M. G. Genton, and D. E. Keyes. ExaGeoStat: A high performance unified framework for geostatistics on manycore systems. *arXiv preprint arXiv:1708.02835*, 2017.
- [2] S. Ambikasaran, D. Foreman-Mackey, L. Greengard, D. W. Hogg, and M. O’Neil. Fast direct methods for Gaussian processes and the analysis of NASA Kepler mission data. *arXiv preprint arXiv:1403.6015*, 2014.
- [3] S. Ambikasaran, J. Y. Li, P. K. Kitanidis, and E. Darve. Large-scale stochastic linear inversion using hierarchical matrices. *Computational Geosciences*, 17(6):913–927, 2013.
- [4] J. Ballani and D. Kressner. Sparse inverse covariance estimation with hierarchical matrices. http://sma.epfl.ch/~anchpcommon/publications/quic_ballani_kressner_2014.pdf, 2015.
- [5] S. Banerjee, A. E. Gelfand, A. O. Finley, and H. Sang. Gaussian predictive process models for large spatial data sets. *Journal of the Royal Statistical Society: Series B (Statistical Methodology)*, 70(4):825–848, 2008.
- [6] M. Bebendorf. Approximation of boundary element matrices. *Numerical Mathematics*, 86(4):565–589, 2000.
- [7] M. Bebendorf. Why approximate LU decompositions of finite element discretizations of elliptic operators can be computed with almost linear complexity. *SIAM J. Numerical Analysis*, 45:1472–1494, 2007.
- [8] M. Bebendorf and T. Fischer. On the purely algebraic data-sparse approximation of the inverse and the triangular factors of sparse matrices. *Numerical Linear Algebra with Applications*, 18(1):105–122, 2011.
- [9] M. Bebendorf and W. Hackbusch. Existence of H-matrix approximants to the inverse FE-matrix of elliptic operators with L^∞ -coefficients. *Numerische Mathematik*, 95(1):1–28, 2003.
- [10] M. Bebendorf and W. Hackbusch. Stabilized rounded addition of hierarchical matrices. *Numerical Linear Algebra Applications*, 14(5):407–423, 2007.

- [11] M. Bebendorf and S. Rjasanow. Adaptive low-rank approximation of collocation matrices. *Computing*, 70(1):1–24, 2003.
- [12] S. Börm and J. Garcke. Approximating Gaussian processes with H^2 -matrices. In J. N. Kok, J. Koronacki, R. L. de Mantaras, S. Matwin, D. Mladen, and A. Skowron, editors, *Proceedings of 18th European Conference on Machine Learning, Warsaw, Poland, September 17-21, 2007. ECML 2007*, volume 4701, pages 42–53, 2007.
- [13] S. Börm and L. Grasedyck. Hybrid cross approximation of integral operators. *Numer. Math.*, 101(2):221–249, 2005.
- [14] S. Börm, L. Grasedyck, and W. Hackbusch. *Hierarchical Matrices*, volume 21 of *Lecture Note*. Max-Planck Institute for Mathematics, Leipzig, 2003. www.mis.mpg.de.
- [15] R. P. Brent. Chapter 4: An algorithm with guaranteed convergence for finding a zero of a function, algorithms for minimization without derivatives. *Englewood Cliffs, NJ: Prentice-Hall*, 1973.
- [16] J. E. Castrillon, M. G. Genton, and R. Yokota. Multi-Level Restricted Maximum Likelihood Covariance Estimation and Kriging for Large Non-Gridded Spatial Datasets. *Spatial Statistics*, 18:105–124, 2016.
- [17] N. Cressie and G. Johannesson. Fixed rank kriging for very large spatial data sets. *Journal of the Royal Statistical Society: Series B (Statistical Methodology)*, 70(1):209–226, 2008.
- [18] A. Datta, S. Banerjee, A. O. Finley, and A. E. Gelfand. Hierarchical nearest-neighbor Gaussian process models for large geostatistical datasets. *Journal of the American Statistical Association*, 0(ja):00–00, 2015.
- [19] M. Fuentes. Approximate likelihood for large irregularly spaced spatial data. *Journal of the American Statistical Association*, 102:321–331, 2007.
- [20] G.-A. Fuglstad, D. Simpson, F. Lindgren, and H. Rue. Does non-stationary spatial data always require non-stationary random fields? *Spatial Statistics*, 14:505–531, 2015.
- [21] R. Furrer, M. G. Genton, and D. Nychka. Covariance tapering for interpolation of large spatial datasets. *Journal of Computational and Graphical Statistics*, 15(3):502–523, 2006.
- [22] G. H. Golub and C. F. Van Loan. *Matrix computations*, 2012.
- [23] S. A. Goreinov, E. E. Tyrtshnikov, and N. L. Zamarashkin. A theory of pseudoskeleton approximations. *Linear Algebra Appl.*, 261:1–21, 1997.
- [24] L. Grasedyck and W. Hackbusch. Construction and arithmetics of \mathcal{H} -matrices. *Computing*, 70(4):295–334, 2003.

- [25] J. Guinness and I. Ipsen. Efficient computation of Gaussian likelihoods for stationary Markov random field models. <http://www4.ncsu.edu/~ipsen/ps/MRFlikelihoods.pdf>, 2015.
- [26] P. Guttorm and T. Gneiting. Studies in the history of probability and statistics XLIX: On the Matérn correlation family. *Biometrika*, 93:989–995, 2006.
- [27] W. Hackbusch. A sparse matrix arithmetic based on \mathcal{H} -matrices. I. Introduction to \mathcal{H} -matrices. *Computing*, 62(2):89–108, 1999.
- [28] W. Hackbusch. *Hierarchical matrices: Algorithms and Analysis*, volume 49 of *Springer Series in Comp. Math.* Springer, 2015.
- [29] W. Hackbusch and B. N. Khoromskij. A sparse \mathcal{H} -matrix arithmetic. II. Application to multi-dimensional problems. *Computing*, 64(1):21–47, 2000.
- [30] W. Hackbusch, B. N. Khoromskij, and R. Kriemann. Hierarchical matrices based on a weak admissibility criterion. *Computing*, 73(3):207–243, 2004.
- [31] M. S. Handcock and M. L. Stein. A Bayesian analysis of kriging. *Technometrics*, 35:403–410, 1993.
- [32] H. Harbrecht, M. Peters, and M. Siebenmorgen. Efficient approximation of random fields for numerical applications. *Numerical Linear Algebra with Applications*, 22(4):596–617, 2015.
- [33] K. L. Ho and L. Ying. Hierarchical interpolative factorization for elliptic operators: differential equations. *Communications on Pure and Applied Mathematics*, 2015.
- [34] H. Huang and Y. Sun. Hierarchical low rank approximation of likelihoods for large spatial datasets. *Journal of Computational and Graphical Statistics*, to appear. *ArXiv e-prints 1605.08898*, 2017.
- [35] I. C. F. Ipsen and D. J. Lee. Determinant approximations. <http://arxiv.org/abs/1105.0437v1>, 2005.
- [36] C. G. Kaufman, M. J. Schervish, and D. W. Nychka. Covariance tapering for likelihood-based estimation in large spatial datasets. *Journal of the American Statistical Association*, 103(484):1545–1555, 2008.
- [37] B. N. Khoromskij and A. Litvinenko. Data sparse computation of the Karhunen-Loève expansion. *AIP Conference Proceedings*, 1048(1):311, 2008.
- [38] B. N. Khoromskij and A. Litvinenko. Domain decomposition based H-matrix preconditioners for the skin problem. *Domain Decomposition Methods in Science and Engineering XVII*, pages 175–182, 2008.
- [39] B. N. Khoromskij, A. Litvinenko, and H. G. Matthies. Application of hierarchical matrices for computing the Karhunen-Loève expansion. *Computing*, 84(1-2):49–67, 2009.

- [40] W. Kleiber and D. W. Nychka. Equivalent kriging. *Spatial Statistics*, 12:31–49, 2015.
- [41] R. Kriemann. Parallel H-matrix arithmetics on shared memory systems. *Computing*, 74(3):273–297, 2005.
- [42] F. Lindgren, H. Rue, and J. Lindström. An explicit link between Gaussian fields and Gaussian Markov random fields: the stochastic partial differential equation approach. *Journal of the Royal Statistical Society: Series B (Statistical Methodology)*, 73(4):423–498, 2011.
- [43] A. Litvinenko. Application of hierarchical matrices for solving multiscale problems. *PhD Dissertation, Leipzig University*, 2006.
- [44] A. Litvinenko. Partial inversion of elliptic operator to speed up computation of likelihood in bayesian inference. *arXiv preprint arXiv:1708.02207*, 2017.
- [45] A. Litvinenko and H. G. Matthies. Sparse data representation of random fields. *PAMM*, 9(1):587–588, 2009.
- [46] A. Litvinenko and H. G. Matthies. Inverse problems and uncertainty quantification. *arXiv preprint arXiv:1312.5048, 2013*, 2013.
- [47] P.-G. Martinsson and V. Rokhlin. A fast direct solver for boundary integral equations in two dimensions. *Journal of Computational Physics*, 205(1):1–23, 2005.
- [48] B. Matérn. *Spatial Variation*, volume 36 of *Lecture Notes in Statistics*. Springer-Verlag, Berlin; New York, second edition edition, 1986.
- [49] H. Matthies, A. Litvinenko, O. Pajonk, B. V. Rosić, and E. Zander. Parametric and uncertainty computations with tensor product representations. In A. M. Dienstfrey and R. F. Boisvert, editors, *Uncertainty Quantification in Scientific Computing*, volume 377 of *IFIP Advances in Information and Communication Technology*, pages 139–150. Springer Berlin Heidelberg, 2012.
- [50] W. Nowak and A. Litvinenko. Kriging and spatial design accelerated by orders of magnitude: combining low-rank covariance approximations with FFT-techniques. *Mathematical Geosciences*, 45(4):411–435, 2013.
- [51] D. Nychka, S. Bandyopadhyay, D. Hammerling, F. Lindgren, and S. Sain. A multiresolution Gaussian process model for the analysis of large spatial datasets. *Journal of Computational and Graphical Statistics*, 24(2):579–599, 2015.
- [52] O. Pajonk, B. V. Rosić, A. Litvinenko, and H. G. Matthies. A deterministic filter for non-Gaussian Bayesian estimation — applications to dynamical system estimation with noisy measurements. *Physica D: Nonlinear Phenomena*, 241(7):775–788, 2012.
- [53] W. H. Press, S. A. Teukolsky, W. T. Vetterling, and B. P. Flannery. *Section 9.3. Van Wijngaarden-Dekker-Brent Method. Numerical Recipes: The Art of Scientific Computing*, volume 3rd ed. New York: Cambridge University Press., 2007.

- [54] J. Quinonero-Candela, C. E. Rasmussen, and R. Herbrich. A unifying view of sparse approximate Gaussian process regression. *Journal of Machine Learning Research*, 6:1939–1959, 2005.
- [55] B. V. Rosić, A. Kučerová, J. Šykora, O. Pajonk, A. Litvinenko, and H. G. Matthies. Parameter identification in a probabilistic setting. *Engineering Structures*, 50:179–196, 2013.
- [56] B. V. Rosić, A. Litvinenko, O. Pajonk, and H. G. Matthies. Sampling-free linear bayesian update of polynomial chaos representations. *Journal of Computational Physics*, 231(17):5761–5787, 2012.
- [57] H. Rue and L. Held. Gaussian Markov random fields: theory and applications, 2005.
- [58] H. Rue and H. Tjelmeland. Fitting Gaussian Markov random fields to Gaussian fields. *Scandinavian Journal of Statistics*, 29(1):31–49, 2002.
- [59] A. Saibaba, S. Ambikasaran, J. Yue Li, P. Kitanidis, and E. Darve. Application of hierarchical matrices to linear inverse problems in geostatistics. *Oil & Gas Science and Technology–Rev. IFP Energies Nouvelles*, 67(5):857–875, 2012.
- [60] H. Sang and J. Z. Huang. A full scale approximation of covariance functions for large spatial data sets. *Journal of the Royal Statistical Society: Series B (Statistical Methodology)*, 74(1):111–132, 2012.
- [61] S. Si, C.-J. Hsieh, and I. S. Dhillon. Memory efficient kernel approximation. In *International Conference on Machine Learning (ICML)*, jun 2014.
- [62] M. L. Stein. Statistical properties of covariance tapers. *Journal of Computational and Graphical Statistics*, 22(4):866–885, 2013.
- [63] M. L. Stein. Limitations on low rank approximations for covariance matrices of spatial data. *Spatial Statistics*, 8:1–19, 2014.
- [64] M. L. Stein, Z. Chi, and L. J. Welty. Approximating likelihoods for large spatial data sets. *Journal of the Royal Statistical Society: Series B (Statistical Methodology)*, 66(2):275–296, 2004.
- [65] Y. Sun, B. Li, and M. G. Genton. Geostatistics for large datasets. In M. Porcu, J. M. Montero, and M. Schlather, editors, *Space-Time Processes and Challenges Related to Environmental Problems*, pages 55–77. Springer, 2012.
- [66] Y. Sun and M. L. Stein. Statistically and computationally efficient estimating equations for large spatial datasets. *Journal of Computational and Graphical Statistics*, 25(1):187–208, 2016.

A Appendix

Theorem 3 Let $\mathbf{C} \in \mathbb{R}^{N \times N}$, and $\mathbf{E} := \mathbf{C} - \tilde{\mathbf{C}}$, $\tilde{\mathbf{C}}^{-1}\mathbf{E} := \tilde{\mathbf{C}}^{-1}\mathbf{C} - \mathbf{I}$, and for the spectral radius $\rho(\tilde{\mathbf{C}}^{-1}\mathbf{E}) = \rho(\tilde{\mathbf{C}}^{-1}\mathbf{C} - \mathbf{I}) < \varepsilon < 1$. Then

$$|\log |\mathbf{C}| - \log |\tilde{\mathbf{C}}|| \leq -n \log(1 - \varepsilon).$$

Proof: See [4]; Ballani and Kressner observed that parameter n in the last inequality is pessimistic and is barely observable in numerical simulations. ■

To prove Theorem 2 we apply Theorem 3 and

$$\begin{aligned} |\tilde{\mathcal{L}}(\boldsymbol{\theta}; k) - \mathcal{L}(\boldsymbol{\theta})| &= \frac{1}{2} \log \frac{|\mathbf{C}|}{|\tilde{\mathbf{C}}|} - \frac{1}{2} |\mathbf{Z}^\top (\mathbf{C}^{-1} - \tilde{\mathbf{C}}^{-1}) \mathbf{Z}| \\ &\leq -\frac{1}{2} \cdot n \log(1 - \varepsilon) - \frac{1}{2} |\mathbf{Z}^\top (\mathbf{C}^{-1}\mathbf{C} - \tilde{\mathbf{C}}^{-1}\mathbf{C}) \mathbf{C}^{-1}\mathbf{Z}| \\ &\leq -\frac{1}{2} \cdot n \log(1 - \varepsilon) - \frac{1}{2} |\mathbf{Z}^\top (\mathbf{I} - \tilde{\mathbf{C}}^{-1}\mathbf{C}) \mathbf{C}^{-1}\mathbf{Z}| \\ &\leq \frac{1}{2} \cdot n\varepsilon + \frac{1}{2} c_0^2 \cdot c_1 \cdot \varepsilon, \end{aligned}$$

where $-\log(1 - \varepsilon) \approx \varepsilon$ for small ε .

Remark A.1 Assumption $\|\mathbf{C}^{-1}\| \leq c_1$ is strong. This estimation depends on the matrix \mathbf{C} , the smoothness parameter ν , the covariance length ℓ , and the \mathcal{H} -matrix rank k . First, we find an appropriate block-decomposition for the covariance matrix \mathbf{C} . Second, we estimate the ranks of $\tilde{\mathbf{C}}$. Third, we prove that the inverse/Cholesky can also be approximated in the \mathcal{H} -matrix format. Then we estimate ranks for the inverse $\tilde{\mathbf{C}}^{-1}$ and the Cholesky factor $\tilde{\mathbf{L}}$. Finally, we estimate the \mathcal{H} -matrix approximation accuracies; see [28]. In the worst case, the rank k will be of order n . We also note that some covariance matrices are singular, so that $\tilde{\mathbf{C}}^{-1}$ and $\tilde{\mathbf{L}}$ may not exist. The computation of $\log |\tilde{\mathbf{C}}|$ could be an ill-posed problem, in the sense that small perturbations in \mathbf{C} result in large changes in $\log |\mathbf{C}|$.

Lemma A.1 Let \mathbf{z} be a vector, where $\|\mathbf{z}\| \leq c_0$, and let $\tilde{\mathbf{L}}^{-1}$ be an \mathcal{H} -matrix approximation of $\tilde{\mathbf{L}}$ such that

$\|\tilde{\mathbf{L}}^{-1} - \tilde{\mathbf{L}}^{-1}\| \leq \varepsilon_L$, and let $\tilde{\mathbf{C}}^{-1}$ be an \mathcal{H} -matrix approximation of \mathbf{C}^{-1} such that $\|\tilde{\mathbf{C}}^{-1} - \mathbf{C}^{-1}\| \leq \varepsilon_C$. Then

$$\|\tilde{\mathbf{L}}^{-1}\mathbf{z} - \mathbf{L}^{-1}\mathbf{z}\| \leq \|\tilde{\mathbf{L}}^{-1} - \mathbf{L}^{-1}\| \cdot \|\mathbf{z}\| \leq c_0 \cdot \varepsilon_L. \quad (5)$$

Proof: Follows from properties of the norm. ■